Polymer Chemistry

PAPER

Hydrolytically degradable poly(β-thioether ester ketal) thermosets *via* radical-mediated thiol–ene photopolymerization†

Cite this: DOI: 10.1039/c9py01082c

Benjamin M. Alameda, Travis C. Palmer, Jonathan D. Sisemore, Nicholas G. Pierini and Derek L. Patton *

Thiol–ene photopolymerization was exploited for the synthesis of poly(β-thioether ester ketal) networks capable of undergoing complete degradation under acid and/or basic conditions. Using the design of four novel bisalkene diketal monomers, we demonstrate the ability to tune degradation profiles under acidic conditions with timescales dictated by the structure of the diketal linker, while hydrolysis of the β-thioether ester functionality dominates the degradation profile under basic conditions irrespective of the diketal structure. All four poly(β-thioether ester ketal) exhibited degradation behavior characteristic of a surface erosion process. The networks showed mechanical (low modulus) and thermomechanical properties (low T_g) typical of thiol–ene thermosets with minimal influence from the structure of the diketal linkage. To highlight the advantages of endowing a step-growth network with ketal linker chemistry, we demonstrated the ability to recover diketone precursors from the thermoset degradation by-products and recycle these compounds into building blocks for additional thermoset materials.

Received 22nd July 2019,
Accepted 1st October 2019

DOI: 10.1039/c9py01082c

rsc.li/polymers

Introduction

Efforts to fabricate crosslinked polymer networks containing labile covalent linkages have enabled the design of degradable materials for potential applications including high performance thermosets,[1] life-changing medical devices,[2] and targeted therapeutic delivery vehicles.[3,4] Each of these applications has specific requirements for shelf-life, performance lifetime, and end of use processing that are closely coupled to the degradation profile of the materials. Degradation profiles are ultimately defined, and in many cases, limited by the nature of the labile covalent chemistry employed in the design of the crosslinker. Hydrolytically labile chemistries such as esters[5,6] and anhydrides[7,8] have been the primary focus for the development of crosslinkers enabling the synthesis of materials that degrade in response to changes in pH, while chemistries based on orthoesters,[9,10] acetals,[11–19] and ketals[12,20–24] have received significantly less attention. Ketals are a particularly attractive option for the design of degradable materials with tunable degradation behavior, as ketals with a broad range of pH-dependent hydrolytic half-lives can be easily obtained from a wide variety of available ketones.[25,26] Ketals exhibit outstanding stability under basic conditions while readily undergoing hydrolysis to yield charge neutral degradation by-products, including the parent ketone and alcohol, when exposed to acidic conditions. This hydrolytic process occurs *via* a well-established mechanism in which the formation of the resonance-stabilized carbenium ion intermediate is the rate determining step.[13,25,26]

Ketals have been used extensively to form various degradable polymer topologies including linear,[20–22,27–30] hyperbranched,[31,32] and star[33] polymers. However, the use of ketals as degradable crosslinkers has received less attention. Ketal-based crosslinkers were initially reported as acid-cleavable crosslinking reagents for proteins in 1989 by Srinivasachar and coworkers.[34] Buchwalter and Kosbar extended the chemistry to polymers in 1996 employing cleavable ketal crosslinkers for the design of acid-degradable thermosets based on cycloaliphatic epoxides.[35] These early reports served as the foundation for continued investigation of ketal-based crosslinkers predominately for degradable drug delivery platforms.[36] Despite a long history, the scope of ketal structures explored as crosslinkers for these degradable applications has been limited mostly to acyclic dimethyl ketals.[12,23,24,33] The dimethyl ketal functionality readily undergoes hydrolysis under mildly acidic conditions but affords little opportunity to tailor the degradation profile for specific environments or applications. Liu and Thayumanavan helped expand this scope by describing the influence of structural variations of 18 different acetal and ketal-

School of Polymer Science and Engineering, The University of Southern Mississippi, Hattiesburg, MS 39402, USA

†Electronic supplementary information (ESI) available: NMR characterization of all monomers; real-time FTIR kinetics for all photopolymerizations. See DOI: 10.1039/c9py01082c

based crosslinkers on degradation kinetics of polymer nanogels.[13] For example, acyclic ketal analogs derived from cyclopentanone and cyclohexanone were found to degrade two to seven times slower than the dimethyl ketal analog. These results provide an opportunity to broadly expand the tunability of polymer degradation profiles but focused entirely on acyclic ketals.

Cyclic ketals offer an additional avenue to pursue crosslinked polymers with tailored degradability; however, these structures have been rarely reported as building blocks for degradable networks. Hu *et al.* reported one of the few examples of spirocyclic ketal diacrylate crosslinkers, enabling exploration of these materials as resists for UV nanoimprint lithography.[37,38] Hu's spirocyclic diketal resin was based on acrylate functionality and chain growth polymerization. It is well established that degradation of a crosslinked polymer network is influenced by network chemistry, crosslink chemistry, and network structure.[39] Networks formed *via* chain growth polymerization of acrylates, for example, are typically heterogeneous (localized regions of high crosslink density interspersed among regions of low crosslink density) due to the formation of various kinetic chain lengths and result in high molecular weight backbones of C–C bonds, rendering much of the material nondegradable – distinct disadvantages in terms of designed degradability. In contrast, step-growth polymerizations provide a route to homogeneous networks with improved control over crosslink density, network structure, and an opportunity to incorporate degradable crosslinks throughout the network eliminating high molecular weight degradation by-products.[39–42]

Herein, we report the synthesis of degradable poly(β-thioether ester ketal) networks *via* thiol–ene photopolymerization of four new bisalkene diketal monomers with a mercaptopropionate-based trifunctional thiol. The diketal monomers were designed from readily available diketones and a commercially available alkenyl-diol. The synthetic route exploits the step-growth nature of thiol–ene photopolymerization to covalently integrate hydrolytically labile diketals into the backbone of the polymer network at each crosslink junction – an approach that yields thermosets that completely degrade into charge neutral ketone and alcohol by-products under acidic conditions. We demonstrate the ability to tune the degradation profile under acidic conditions with timescales dictated by the structure of the diketal linker, while hydrolysis of the β-thioether ester functionality dominates the degradation profile under basic conditions irrespective of the diketal structure. We also highlight the potential to recover and reuse the diketone degradation by-product to regenerate a new batch of bisalkene diketal monomer for synthesis of additional poly(β-thioether ester ketal) materials.

Experimental

Materials

All reagents were obtained commercially and used without further purification unless otherwise specified. 1,4-Diacetylbenzene, 4,4′-bicyclohexanone and 3-allyloxy-1,2-propanediol were sourced from TCI Chemical. 2,3-Butanedione was sourced from Alfa Aesar; 1,4-cyclohexanedione was sourced from Acros; ethoxylated trimethylolpropane tri(3-mercaptopropionate) (ETTMP 1300) was sourced from Bruno Bock; Darocur 1173 was sourced from Ciba; p-toluenesulfonic acid (p-TsOH) and benzene was sourced from Sigma Aldrich. All other solvents were obtained from Fisher Scientific.

Monomer characterization

Monomer structure was confirmed by mass spectrometry using a Bruker 12 Tesla APEX – Qe FTICR-MS in positive-ion mode ionization with an Apollo II ion source. Monomer structure and purity was additionally confirmed by ^{1}H NMR, ^{13}C NMR, COSY and HSQC experiments using a Bruker Avance™ 600 MHz NMR in deuterated chloroform.

Synthesis of monomer 3

1,4-Cyclohexanedione (6.60 g, 58.9 mmol, 1 eq.), 3-allyloxy-1,2-propanediol (49.0 g, 371 mmol, 6.30 eq.), and 0.1 mol% of p-TsOH were dissolved in 40.0 mL benzene and refluxed for 6 h using a Dean–Stark apparatus. The reaction mixture was washed 3 times with saturated $NaHCO_3$ and again 3 times with brine. The organic layer was dried over $MgSO_4$, filtered and rotary evaporated to yield the crude product. The crude product was then dissolved in a minimal amount of methylene chloride and further purified using column chromatography using 10 : 90 acetone : hexanes + 3% triethylamine as the eluent. The collected fraction was rotary evaporated and left under vacuum for 6 h to yield 17.2 g of the final product (yield: 85.9%). ^{1}H NMR (600 MHz, $CDCl_3$) δ 5.91 (ddt, J = 17.3, 10.4, 5.6 Hz, 2H), 5.29 (dt, J = 17.2, 1.6 Hz, 2H), 5.21 (dd, J = 10.4, 1.5 Hz, 2H), 4.29 (p, J = 6.0 Hz, 2H), 4.10–4.01 (m, 6H), 3.78 (dd, J = 8.3, 6.3 Hz, 2H), 3.57–3.54 (m, 2H), 3.46 (ddd, J = 9.8, 5.6, 3.6 Hz, 2H), 1.91–1.75 (m, 8H). ^{13}C NMR (151 MHz, $CDCl_3$) δ 134.51 (CH), 117.25 (CH_2), 109.02 (C), 74.61 (CH_2), 74.56 (CH_2), 72.48 (CH_2), 71.10 (CH_2), 71.07 (CH_2), 66.75 (CH_2), 66.71 (CH_2), 33.46 (CH_2), 33.29 (CH_2), 33.27 (CH_2), 31.95 (CH_2), 31.79 (CH_2), 31.74 (CH_2). HRMS (ESI): calcd for $C_{18}H_{28}O_6Na^+$ $[M + Na]^+$ m/z: 363.177810, found: 363.177735.

Synthesis of monomer 5

4,4′-Bicyclohexanedione (1.01 g, 5.20 mmol, 1 eq.), 3-allyloxy-1,2-propanediol (6.00 g, 45.0 mmol, 8.65 eq.), and 0.1 mol% of p-TsOH were dissolved in 55.0 mL benzene and refluxed for 6 h using a Dean–Stark apparatus. The reaction mixture was washed 3 times with saturated $NaHCO_3$ and again 3 times with brine. The organic layer was dried over $MgSO_4$, filtered and rotary evaporated to yield the crude product. The crude product was then dissolved in a minimal amount of methylene chloride and further purified using column chromatography using 20 : 80 acetone : hexanes + 3% triethylamine as the eluent. The collected fraction was rotary evaporated and left under vacuum for 6 h to yield 1.05 g of the final product (yield: 47.8%). ^{1}H NMR (600 MHz, $CDCl_3$) δ 5.94–5.85 (m, 2H), 5.31–5.23 (m, 2H), 5.18 (d, J = 10.4 Hz, 2H), 4.30–4.20 (m, 2H),

4.08–3.98 (m, 6H), 3.75 (dd, J = 7.8, 6.5 Hz, 1H), 3.74–3.68 (m, 1H), 3.57–3.49 (m, 2H), 3.45–3.41 (m, 2H), 1.85–1.76 (m, 2H), 1.75–1.63 (m, 6H), 1.63–1.51 (m, 2H), 1.50–1.21 (m, 6H), 1.19–1.08 (m, 2H). ^{13}C NMR (151 MHz, $CDCl_3$) δ 134.59 (CH_2), 134.53 (CH_2), 117.25 (CH), 117.13 (CH), 110.00 (C), 109.80 (C), 74.50 (CH), 74.28 (CH), 72.49 (CH_2), 72.44 (CH_2), 71.34 (CH_2), 71.21 (CH_2), 66.70 (CH_2), 66.59 (CH_2), 41.23 (CH), 41.00 (CH), 36.16 (CH_2), 36.00 (CH_2), 34.63 (CH_2), 34.50 (CH_2), 27.58 (CH_2), 27.52 (CH_2), 27.47 (CH_2), 27.45 (CH_2), 27.35 (CH_2), 27.30 (CH_2), 27.25 (CH_2), 27.23 (CH_2), 27.20 (CH_2), 27.17 (CH_2). HRMS (ESI): calcd for $C_{24}H_{38}O_6Na^+$ $[M + Na]^+$ m/z: 445.256060, found: 445.255849.

Synthesis of monomer 7

2,3-Butanedione (5.48 g, 63.7 mmol, 1 eq.), 3-allyloxy-1,2-propanediol (33.0 g, 250 mmol, 3.76 eq.), and 0.1 mol% of p-TsOH were dissolved in 55.0 mL benzene and refluxed for 4 h using a Dean–Stark apparatus. Any organic layer collected in the Dean–Stark trap was transferred back to the reaction vessel throughout the reaction process. The reaction mixture was washed 3 times with saturated $NaHCO_3$ and again with 3 times with brine. The organic layer was dried over $MgSO_4$, filtered and rotary evaporated to yield the crude product. The crude product was then dissolved in a minimal amount of methylene chloride and further purified using column chromatography using 20 : 80 acetone : hexanes + 3% triethylamine as the eluent. The collected fraction was rotary evaporated and left under vacuum for 6 h to yield 11.4 g of the final product (yield: 57.1%). ^{1}H NMR (600 MHz, $CDCl_3$) δ 5.94–5.82 (m, 2H), 5.31–5.22 (m, 2H), 5.22–5.14 (m, 2H), 4.51–4.46 (m, 0.5H), 4.46–4.39 (m, 0.5H), 4.16–4.10 (m, 0.5H), 4.08 (dd, J = 11.6, 7.4 Hz, 0.5H), 4.05–3.90 (m, 6H), 3.85–3.74 (m, 1H), 3.72–3.59 (m, 1H), 3.58–3.46 (m, 2.5H), 3.46–3.37 (m, 1.5H), 1.48–1.34 (m, 6H). ^{13}C NMR (151 MHz, $CDCl_3$) δ 134.51 (CH), 117.05 (CH_2), 96.45 (C), 96.11 (C), 96.00 (C), 95.73 (C), 95.64 (C), 95.36 (C), 95.12 (C), 95.04 (C), 94.50 (C), 72.52 (CH_2), 72.46 (CH_2), 72.35 (CH_2), 71.40 (CH_2), 71.36 (CH_2), 70.81 (CH_2), 70.70 (CH_2), 70.64 (CH_2), 70.18 (CH_2), 70.06 (CH_2), 69.55 (CH_2), 69.50 (CH_2), 68.65 (CH_2), 68.18 (CH_2), 66.27 (CH_2), 66.18 (CH_2), 65.89 (CH_2), 65.82 (CH_2), 64.47 (CH_2), 64.07 (CH_2), 62.91 (CH_2), 61.23 (CH_2), 61.15 (CH_2), 25.49 (CH_3), 23.51 (CH_3), 22.05 (CH_3), 20.68 (CH_3), 20.45 (CH_3), 20.27 (CH_3), 19.95 (CH_3), 19.77 (CH_3).

HRMS (ESI): calcd for $C_{16}H_{26}O_6Na^+$ $[M + Na]^+$ m/z: 337.162160, found: 337.161980.

Synthesis of monomer 9

1,4-Diacetylbenzene (6.71 g, 41.4 mmol, 1 eq.), 3-allyloxy-1,2-propanediol (24 g, 182 mmol, 4.39 eq.), and 0.1 mol% of p-TsOH were dissolved in 55.0 mL benzene and refluxed for 6 h using a Dean–Stark apparatus. The reaction mixture was washed 3 times with saturated $NaHCO_3$ and again 3 times with brine. The organic layer was dried over $MgSO_4$, filtered and rotary evaporated to yield the crude product. The crude product was then dissolved in a minimal amount of methylene chloride and further purified using column chromatography using 15 : 85 acetone : hexanes + 5% triethylamine as the eluent. The collected fraction was rotary evaporated and left under vacuum for 6 h to yield 6.17 g of the final product (yield: 38.2%). ^{1}H NMR (600 MHz, chloroform-d) δ 7.48–7.42 (m, 4H), 5.95–5.80 (m, 2H), 5.28 (dd, J = 17.2, 1.6 Hz, 1.5H), 5.24–5.17 (m, 2H), 5.16–5.12 (d, 0.5H), 4.42 (quint, J = 7.5, 6.1 Hz, 0.5H), 4.19 (dd, J = 8.4, 6.3 Hz, 0.5H), 4.14 (quint, J = 5.9 Hz, 1.5H), 4.10–4.02 (m, J = 5.7, 4.2, 1.4 Hz, 3H), 4.00–3.91 (m, 1H), 3.81 (d, J = 6.1 Hz, 3H), 3.60 (m, 1.5H), 3.57 (t, J = 8.4, 7.4 Hz, 0.5H), 3.53–3.44 (m, 2H), 3.27 (dd, J = 9.9, 5.7, 0.9 Hz, 0.5H), 1.66 (s, J = 2.0 Hz, 4.5H), 1.63 (s, J = 1.9 Hz, 1.5H). ^{13}C NMR (151 MHz, $CDCl_3$) δ 143.77 (C), 143.72 (C), 142.95 (C), 142.87 (C), 134.51 (CH), 134.45 (CH), 125.15 (CH), 125.03 (CH), 124.91 (CH), 117.33 (CH_2), 117.21 (CH_2), 109.57 (C), 75.64 (CH), 74.63 (C), 72.50 (CH_2), 72.39 (CH_2), 71.19 (CH_2), 70.95 (CH_2), 67.59 (CH_2), 66.87 (CH_2), 28.25 (CH_3), 27.87 (CH_3).

HRMS (ESI): calcd for $C_{22}H_{30}O_6Na^+$ $[M + Na]^+$ m/z: 413.193460, found: 413.193269.

Thermoset preparation

Monomer and ETTMP 1300 were added at a 1 : 1 ratio (alkene : thiol) with 5 mol% Darocur 1173 photoinitiator. The solution was mixed well and degassed under high-vacuum for 5 s, 3 times and transferred to a PDMS mold where 7.00 mm × 3.75 mm thermoset disks of approximately 160 mg were photopolymerized after exposure to a medium pressure 10 mW cm^{-2} UV-lamp for 3 min. All monomers were miscible with ETTMP 1300; however, monomer **9** and ETTMP 1300 had to be preheated to 50.0 °C to fully solubilize.

Photopolymerization kinetics

Polymerization kinetics were measured by real-time FTIR (RT-FTIR) spectroscopy using a Nicolet 8700 FTIR spectrometer with a KBr beam splitter and MCT/A detector. Each sample was exposed to a UV light with an intensity of 100 mW cm^{-2} using an Omnicure Series 1000 light source. Series scans were recorded at approximately 2 scan s^{-1} with a resolution of 4 cm^{-1}. Thiol conversion was monitored by integrating the peak at 2557 cm^{-1} over time, while the conversion of the allyl unsaturated group was monitored by integration of the 1646 cm^{-1} peak. Each experiment consisted of mixing each monomer with ETTMP 1300 (1 : 1 thiol : alkene) and 5 mol% Darocur 1173. Each composition was mixed was using a vibratory mixer and degassed for 5 s under high vacuum 3 times before being sandwiched between two salt plates using 1 drop of resin. Data acquisition and UV exposure were initiated simultaneously and were stopped after 1 min.

Hydrolytic degradation experiments

7.00 mm × 3.75 mm (diameter × thickness) thermoset disks were weighed separately and placed in individually weighed glass vials with 20.0 mL of degradation solution. At specific time intervals, degradation media was decanted from the vials, washed three times with DI water, and then filled with LN_2 to freeze the polymer sample before being transferred to a lyophilizer for 48 h. The dry weight of the sample was then measured

via a microbalance and directly compared to the initial sample weights to obtain the percent mass loss. This method was done in triplicate for each time interval to construct an average residual wt% *vs.* time curve.

Monomer recovery experiment

In a 250 mL round bottom flask, 8.80 g of **9P** was added and filled with 1 M HCl. After being left to degrade overnight, fine white crystals formed at the bottom of the flask. The solution was decanted from the flask and the remaining crystals were washed with deionized water and dried under vacuum to yield 0.855 g of 1,4-diacetylbenzene (**8**). The original round bottom flask was rinsed with deionized water and the 0.855 g of product was transferred back to flask with 2.79 g of 3-allyloxy-1,2-propanediol (**1**), 40 mL benzene and a catalytic amount of p-TsOH. The solution was then refluxed using a Dean–Stark apparatus for 4 h and worked up in the same manner as described previously to yield 1.47 g of monomer **9**. All of monomer **9** was combined with a stoichiometric amount of ETTMP 1300 and 5 mol% Darocur 1173 and photopolymerized to yield 4.78 g of product (**9P**) (total yield 54.3%).

Dynamic mechanical analysis

DMA experiments were conducted on a TA Instruments Q800 using samples of approximate dimensions of 20.0 mm × 5.00 mm × 1.00 mm (length × width × thickness). DMA bar samples were prepared using a PDMS mold, photopolymerized after exposure to a medium pressure UV lamp (10 mW cm^{-2}) for 3 min and stored in a desiccator to prevent any water uptake. Experiments consisted of a temperature sweep from −90.0 °C to 75.0 °C using a constant frequency of 1.0 Hz, a strain rate of 0.05% and a 2.0 °C min^{-1} ramp rate in tensile mode. The glass transition temperature for each sample was measured at the tan delta peak maximum. All experiments were performed in triplicate to ensure consistent sample measurements.

Thermogravimetric analysis

TGA experiments were performed on a TA Instruments Q500 using a platinum pan and 5 μL thermoset disk samples of approximately 7.50 mg. Each experiment consisted of a temperature ramp of 10 °C min^{-1} up to a final temperature of 600 °C in air atmosphere conditions.

Mechanical testing

Tensile testing was conducted in accordance with ASTM D638 utilizing a Type V tensile bar with a gauge length of 7.62 mm, gauge width of 3.18 mm and overall thickness of 1.41 mm. Samples were prepared by photopolymerizing resin formulations in a Type V PDMS mold covered with a glass slide. After exposure to a medium pressure 10 mW cm^{-2} UV-lamp for 3 min, samples were stored in a desiccator until testing to prevent water uptake. The samples were tested on an MTS Insight electromechanical test frame with a 500 N load cell at a constant crosshead speed of 1.52 mm min^{-1} to failure. Testing of each thermoset type was performed in at least triplicate to ensure consistent and accurate measurements.

Results and discussion

Monomer synthesis

Initially, we focused on the synthesis of ketal-containing monomers derived from 1,4-cyclohexanedione (**2**), 4,4′-bicyclohexanone (**4**), 2,3-butanedione (**6**), and 1,4-diacetylbenzene (**8**). Although these diketones are relatively common and, in some cases, derived from renewable sources, they have received minimal attention as building blocks for degradable polymers.[37,38] Du Prez and coworkers[43] recently reported the synthesis of diol monomers containing cyclic ketals derived from the reaction of glycerol with either 1,4-cyclohexadione (**2**) or 4,4′-bicyclohexadione (**4**) as building blocks for linear polyurethanes, polyesters, and polycarbonates. While 2–3-butanedione (**6**) was mentioned by Du Prez *et al.* as a possible monomer precursor, it was abandoned due to slow ketalization kinetics and low yields.[43] A thorough search for examples using 1,4-diacetylbenzene (**8**) as a precursor for ketal-containing monomers yielded no results. In the current work, bisalkene diketal monomers (**3**, **5**, **7**, and **9**) were synthesized using a Dean–Stark apparatus *via* a one-step acid-catalyzed ketalization using 3-allyloxy-1,2-propanediol (**1**) and the series of diketones as building blocks (Fig. 1). Acceptable monomer yields were obtained after purification (**3**, 86%; **5**, 48%; **7**, 57%; **9**, 38%). The lower yield for monomer **9** is attributed to its relative sensitivity towards hydrolysis during the work up procedure. The structure and purity of all monomers were confirmed by ^{1}H NMR, ^{13}C NMR, COSY, HSQC and HRMS (Fig. S1–S16, ESI†). As an example, the ^{1}H and ^{13}C NMR spectra for monomer **3** are shown in Fig. 2. ^{1}H NMR peak integrations showed expected values between the unsaturated allyl protons (A, B), the ether/ketal ring protons (C, D, E, F), the cyclohexyl protons (G, H, I, J) and confirmed an average of 2 unsaturated groups per parent cyclohexyl structure. ^{13}C NMR was employed to identify and confirm specific carbon signals present in the

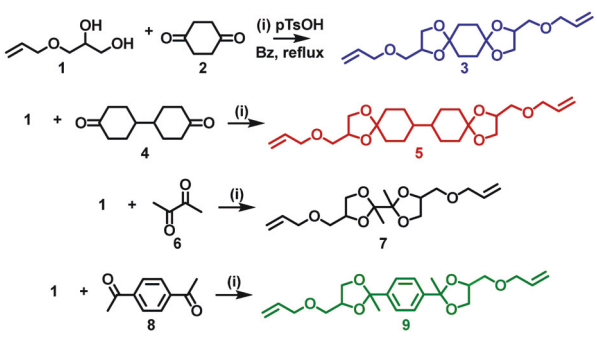

Fig. 1 General synthetic scheme for cyclic ketal monomers **3**, **5**, **7** and **9** from the acid-catalyzed ketalization of diketones (**2**, **4**, **6**, and **8**) and 3-allyloxy-1,2-propanediol (**1**).

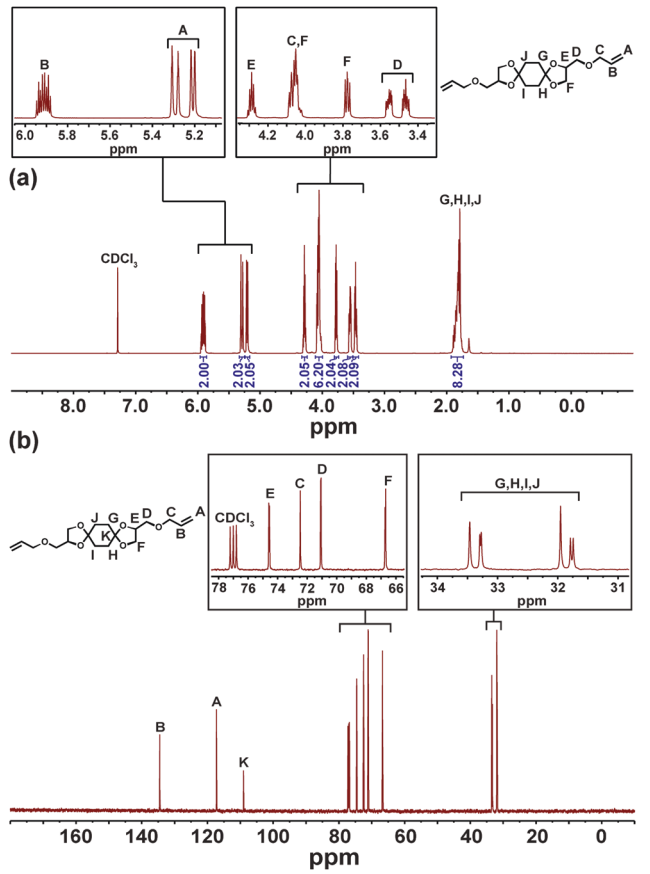

Fig. 2 (a) ^{1}H NMR and (b) ^{13}C NMR spectra of monomer **3** with their respective chemical signal assignments and integration values.

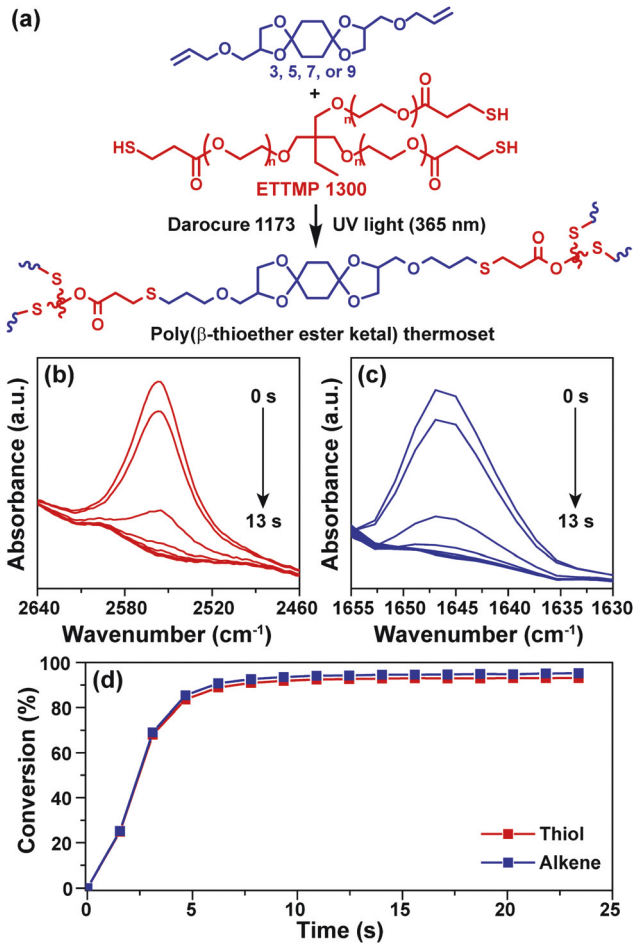

Fig. 3 (a) Thermoset synthetic scheme starting with a generic diketal monomer (representative of monomers **3**, **5**, **7**, or **9**), ETTMP 1300 trifunctional thiol and Darocur 1173 photoinitiator. Change in FTIR peak area for (b) thiol and (c) alkene for monomer **3** and ETTMP 1300 as a function of time. (d) Conversion of thiol and alkene as a function of time for **3** and ETTMP 1300.

product structure such as allyl carbons (A, B) at 134.52 and 117.25 ppm, quaternary carbons (K) at 109.02 ppm, ether and ketal carbons (C, D, E, F) between 75 and 65 ppm and cyclohexyl carbons (G, H, I, J) between 34 and 31 ppm. Multiple peaks were observed for some carbons and is attributed to the formation of product stereoisomers during synthesis. The complex and asymmetric splitting seen for protons C, D, E and F in the ^{1}H NMR was further investigated using COSY and (^{1}H–^{13}C) HSQC experiments in which proper assignments were given to each, with the F protons being responsible for the asymmetric splitting that overlaps with the C proton signal. HSQC experiments also confirmed the carbon assignments by matching them to their respective proton signals. Similar NMR experiments were employed to elucidate the structures of monomers **5**, **7** and **9**.

Photopolymerization and polymer network characterization

Degradable poly(β-thioether ester ketal) thermosets were synthesized *via* thiol–ene photopolymerization using the bisalkene diketal monomers (**3**, **5**, **7**, and **9**) and a commercially available trifunctional thiol. Fig. 3a illustrates a representative solvent-free UV photopolymerization (λ_{max} = 365 nm) using the dialkene diketal monomers, ETTMP 1300, and Darocur 1173 (5 mol%) as the photoinitiator. Resins were formulated with vortex mixing using a 1 : 1 thiol/alkene mole stoichiometry. Bisalkene diketal monomers **3**, **5**, and **7** were fully miscible with ETTMP 1300 at ambient temperatures; only monomer **9** required 10 min of heating at 50 °C to prepare a fully miscible resin. To elucidate the required time of UV exposure to achieve or approach maximum functional group conversion, we followed the polymerization process using real-time FTIR spectroscopy. Polymerization kinetics were measured by exposing the resins to UV light (100 mW cm^{-2}) while simultaneously following the change in thiol (2557 cm^{-1}, Fig. 3b) and alkene (1646 cm^{-1}, Fig. 3c) peak areas over time. A representative kinetic profile for the **3**/ETTMP system is shown in Fig. 3d. Thiol and alkene conversions surpassed >90% in less than 10 s, while maintaining a 1 : 1 thiol to alkene stoichiometry. The stoichiometric consumption of alkene and thiol suggests minimal chain-growth homopolymerization of the alkene and absence of any deleterious side reactions between the thiol and ketal functionality. Similar kinetic profiles and functional

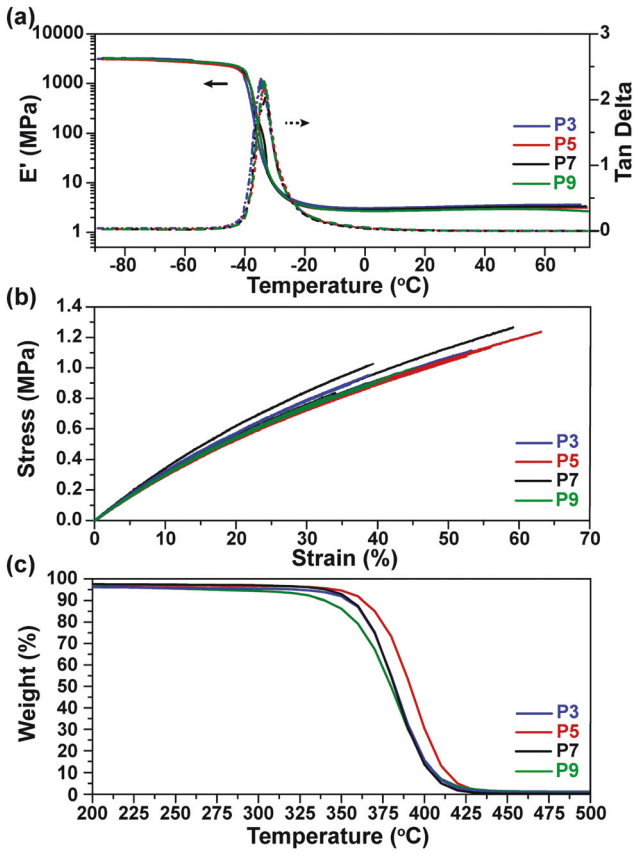

Fig. 4 (a) Storage modulus and tan δ measurements for **P3**, **P5**, **P7** and **P9** obtained by dynamic mechanical analysis. (b) Tensile testing of **P3**, **P5**, **P7** and **P9** using ASTM D638 standard testing methods. (c) Thermogravimetric analysis of **P3**, **P5**, **P7** and **P9** obtained under air atmosphere conditions.

group conversions were observed for all other monomers with ETTMP 1300, as shown in Fig. S17a–d.†

The influence of the various diketal linkers on the thermomechanical and mechanical properties of the poly(thioether ketal) networks was investigated using dynamic mechanical analysis and tensile testing, respectively. Samples were subjected to a small oscillatory strain as a function of temperature to resolve the storage modulus (E'), loss modulus (E'') and tan δ (E'/E''). Fig. 4a shows the tan δ and E' curves for networks derived from monomers **3**, **5**, **7**, and **9** with ETTMP 1300. Narrow tan δ distributions (<9 °C at fwhm) were observed for all thermosets – a typical characteristic of the step-growth thiol–ene polymerization process indicative of homogeneous polymer networks.[44,45] Glass transition temperatures were determined from the peak maximum of the tan δ curves. As shown in Fig. 4a, the glass transition for all four networks was well below 0 °C (specific values summarized in Table 1) and essentially independent of the structure of the ketal linker, suggesting that the T_g is dictated primarily by the flexible thioether linkages common to each of the poly(β-thioether ester ketal) networks. DMA also showed glassy storage moduli in the range of 3000 MPa and a flat, rubbery plateau region for each thermoset that indicated rubbery moduli of approximately 3 MPa at 25 °C (Table 1). Fig. 4b shows an overlay of three stress–strain curves for each of the poly(β-thioether ester ketal) thermosets; quantified values for Young's modulus, strain at break, *etc.* are summarized in Table 1. While the Young's moduli are not observed to change dramatically between the samples, the **5**/ETTMP system demonstrated a measurable increase in strain at break, peak load and peak stress. Most impacted was the strain at break (56.94% *vs.* 40–43% for **P3**, **P7**, and **P9**). We believe the increase in mechanical performance of **P5** is due to its bicyclohexyl structure, which can absorb energy *via* ring flip transitions (*e.g.* boat to chair), a distortional energy absorbing mechanism.[46] Overall, however, we speculate that because the ETTMP 1300 trifunctional thiol makes up for the majority of the network by mass, it dictates the bulk physical properties of the thermoset with minimal influence from the dialkene monomer structure.

Thermogravimetric analysis was employed to characterize the thermal stability of the poly(β-thioether ester ketal) thermosets under air atmosphere conditions. Fig. 4c shows the thermal degradation profiles for each network type and were found to exhibit similar mass loss behavior with relatively high resistance to thermal degradation typical of thioether based networks. The temperature at which 10% mass loss occurs ($T_{d,10}$) was found to be between 339 °C and 364 °C with **9P** having the lowest onset degradation temperature and **5P** the highest (Table 1). A single mass loss transition was observed for all samples and complete degradation occurring with no appreciable char or residue remaining in the TGA pan.

Table 1 Summary of mechanical, thermomechanical and thermal degradation data

	Thermoset			
Property	**3P**	**5P**	**7P**	**9P**
Young's modulus (MPa)	0.0322 ± 0.00136	0.0306 ± 0.000917	0.0306 ± 0.00126	0.0323 ± 0.000737
Strain at break (%)	41.7 ± 7.83	56.9 ± 4.87	43.3 ± 10.9	40.2 ± 6.07
Peak stress (MPa)	0.96 ± 0.11	1.15 ± 0.081	1.01 ± 0.19	0.92 ± 0.094
Peak load (N)	4.30 ± 0.51	4.74 ± 0.40	4.13 ± 0.77	3.62 ± 0.36
T_g, DMA (°C)	−34.6	−33.5	−35.6	−33.8
Glassy modulus 80 °C (MPa)	3237	3052	3131	3131
Rubbery modulus 25 °C (MPa)	3.277	2.934	2.928	2.699
$T_{d,10}$ (°C)	355.3	363.5	356.4	339.9

Polymer network degradation

As illustrated in Fig. 3a, poly(β-thioether ester ketal) networks in this work contain two functional groups – ketals and β-thioether esters – that are susceptible to hydrolytic degradation. In general, ketals are stable under basic conditions but readily undergo acid-catalyzed hydrolysis with rates dictated by the structure of the ketal. The β-thioether ester functionality, on the other hand, is susceptible to hydrolysis under both acidic and basic conditions.[47,48] As a control, we synthesized polymer networks devoid of the ketal functionality from 1,5-hexadiene and ETTMP 1300 (denoted as **PHD**) and compared the degradation behavior of these ester-only thermosets with the poly(β-thioether ester ketal) networks. Prior to discussion of degradation behavior, it is worth noting that all four diketal-based networks and the ester-only control network exhibited similar hydrophobicity as indicated by similar static water contact angle values (*e.g.*, average static WCA of all networks was 40° ± 5°). The hydrophilic character of ETTMP results in observed swelling of these networks in aqueous media (Video S1†), but the general differences in hydrophobicity of the network likely contribute minimally to the observed trends in degradation profiles. We investigated the degradation behavior of the networks by following the mass loss as a function of time in aqueous media at pH 0.2 (HCl/H_2O), pH 7.4 (PBS buffer) and pH 13.5 ($NaOH/H_2O$) under ambient temperature conditions (Fig. 5a). At pH 7.4, the degradation profiles for all thermoset compositions (**P3–P7** and **PHD**) showed no appreciable degradation with negligible mass loss (<5 wt%) over a 120 h period (Fig. 5a). This observation is attributed to the relative stability of both cyclic ketals and esters under neutral aqueous conditions.

In acidic conditions, the degradation profiles shown in Fig. 5a highlight a strong influence of the ketal structure on degradation behavior. For example, an immediate onset of degradation was observed for the **P9** thermosets derived from the 1,4-diacetylbenzene-based diketal and sample pucks were completely degraded within 8 h. In contrast, **P7** thermosets derived from the 2,3-butandione-based diketal exhibited a 6 h induction period and required 20 h to fully degrade. The induction period for **P7** is accompanied by an observed swelling of the material – a time during which the aqueous media diffuses into the surface region of the thermoset with minimal hydrolysis, and consequently, negligible mass loss. The different timescales for degradation of these thermosets can be explained by considering the mechanism for ketal hydrolysis. For **P9**, the aromatic structure of the ketal linker stabilizes the carbocation transition state promoting rapid hydrolysis of the network *via* the ketal functionality. The inductively withdrawing nature of the adjacent ketals in **P7** destabilizes the transition state decreasing the rate of ketal hydrolysis. In fact, the **P7** thermoset closely mirrors the onset and degradation behavior observed for the ester-only control material, indicating that degradation of the **P7** network likely proceeds *via* a competitive process involving both ketal and ester hydrolysis. In the absence of strong electronic effects on the ketal structure, thermosets **P3** and **P5** exhibited short induction periods (<2 h) and intermediate times to full degradation – 14 h for **P3** and 16 h for **P5**. While the difference between the degradation profiles of **P3** and **P5** thermosets is difficult to pinpoint given the similarity of the ketal linkers, we can infer that because the ketal linker derived from monomer **3** has both cyclic ketals on a single central cyclohexyl ring, it would be conformationally more difficult to undergo the sp^3 to sp^2 transition required during the rate determining step of the hydrolysis, thus exhibiting a slightly longer degradation time than **P5**. It should also be noted that as the ketal increases in hydrolytic stability, degradation *via* ester-hydrolysis becomes more competitive (as previously discussed for **P7**).

Under basic conditions, as shown in Fig. 5a, all four poly (β-thioether ester ketal) thermosets were fully degraded in less than 5 h with degradation profiles that were essentially identical to the degradation profile of the ester-only thermoset. These results suggest that ester hydrolysis, irrespective of the ketal structure, is the dominate mechanism of degradation under basic conditions. To further investigate the differences in degradation mechanisms under acidic and basic conditions, the degradation by-products of **P9** were collected after acidic (pH 0.2) and basic conditions (pH 13.5). The major degradation products obtained under acidic conditions were confirmed by ^1H NMR (Fig. S18 and 19†) to be diketone **8** and a multifunctional alcohol, both infer a ketal hydrolysis-controlled degradation mechanism. In contrast, but as expected, the major degradation products obtained from **P9** degradation under basic conditions were confirmed by ^1H NMR as trimethylol propane ethoxylate and a carboxylic acid end-functionalized ketal crosslinker (Fig. S20†), both resulting from an ester hydrolysis-controlled degradation mechanism.

Polymer erosion can be divided into bulk erosion and surface erosion – processes that depend on complex set of variables including hydrolysis rate, diffusion rate (aqueous media into the material, degradation by-products out), hydrophobi-

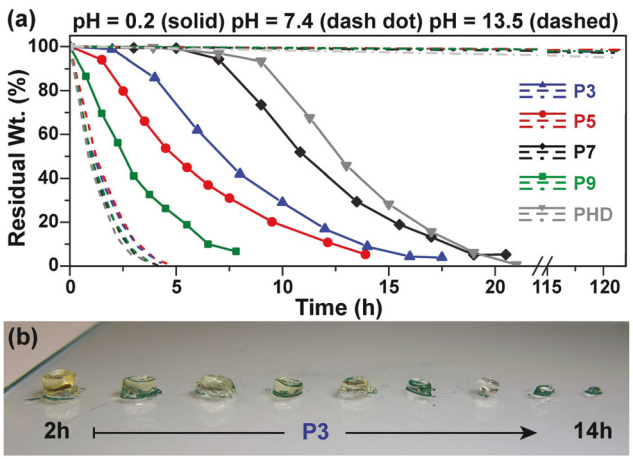

Fig. 5 (a) Mass loss for **P3**, **P5**, **P7**, **P9** and PHD thermoset disks in acidic, (pH: 0.2) PBS buffer (pH: 7.4) and basic (pH: 13.5) solutions as a function of time. (b) Photograph of **P3** thermoset disk at different degradation times.

city, and sample dimensions among others.[49] In general, bulk erosion is dominant when diffusion of water into the polymer is faster than the rate of hydrolysis, since the degradation process is not restricted to the surface. However, surface erosion dominates when the opposite is true – a higher rate of hydrolysis relative to diffusion of water into the material confines the degradation process to the surface. Fig. 5b provides insight into the erosion mechanism of the **P3** thermoset under acidic conditions. Snapshots of the **P3** sample pucks (after freeze drying) show a general retention of shape that decrease in size as a function of degradation time – behavior that is characteristic of a surface erosion process. While all four ketal-based thermosets showed similar behavior in these *ex situ* snapshots, evidence of a mixed-mode erosion process can be observed in the real-time degradation video (Video S1,† note: sample dimensions are smaller for video microscope experiments compared to samples for mass loss experiments) – particularly for the most stable **P7** thermoset. For **P7**, bulk erosion appears to compete and perhaps dominate the surface erosion following the swelling induction period. This mixed mode erosion is likely attributed to both the hydrophilicity of ETTMP and to the relative stability of the ketal/ester under acid conditions. A more hydrophobic and/or ester-free multifunctional thiol could be employed to shift the erosion process to a purely surface erosion mechanism, albeit at the expense of longer overall degradation times.

Monomer precursor recovery experiment

As indicated in Fig. 3a, the step-growth characteristics of thiol–ene photopolymerization installs a hydrolytically labile ketal linkage at each crosslink junction within the polymer network. Complete hydrolysis of the poly(β-thioether ester ketal) thermosets under acidic conditions should therefore result several low molecular weight degradation by-products, including the parent diketone and a multifunctional alcohol. In networks where ester hydrolysis competes with hydrolysis of the ketal, carboxylic acid by-products would also be expected. During our mass loss experiments under acidic conditions, the formation of fine white crystals was observed at the bottom of the flask upon complete degradation of the **P9** thermoset. The crystals were collected, and the structure was confirmed to be 1,4-diacetylbenzene by ^{1}H NMR (Fig. S19†). Recognizing this observation as a potential route to pursue monomer precursor recyclability, we examined the acid-catalyzed degradation of an 8.80 g sample of the **P9** thermoset. The diketone degradation by-product was collected by a simple decantation, washed with deionized water, and dried under vacuum. The pure 1,4-diacetylbenzene was again used for the synthesis of monomer **9**, which was then photopolymerized with ETTMP 1300 to yield 4.80 g of the **P9** thermoset for a total yield of 54.3% (Fig. 6). Even in the absence of process optimization, this recycling approach proved to be easy and relatively efficient. While we only explored the recycling approach for the **P9** thermoset in the current manuscript, a similar process could be adapted for the other poly(β-thioether ester ketal) thermosets but would require a more involved separation to recover the diketone starting materials.

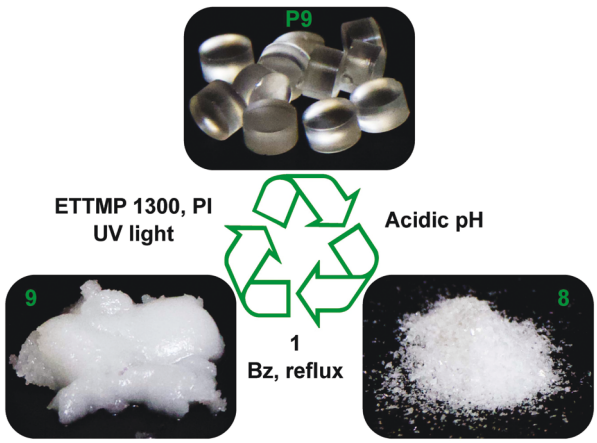

Fig. 6 Recycling of degradation by-product diketone **8** into a new batch of monomer **9** after degradation of thermoset **P9** under acidic conditions.

Conclusions

In this work, we have reported the synthesis of four new bisalkene diketal monomers using a series of common diketones and a commercially available alkenyl-diol under classic acid-catalyzed ketalization conditions. Using radical-mediated thiol–ene photopolymerization, these monomers were combined with an ester-containing multifunctional thiol to yield poly(β-thioether ester ketal) thermosets with tunable degradation profiles under acidic conditions. The resulting thermosets showed mechanical (low modulus) and thermomechanical properties (low T_g) typical of thiol–ene thermosets with minimal influence from the structure of the diketal linkage. The diketal structure, however, significantly influenced the degradation behavior of the poly(β-thioether ester ketal) thermosets under acidic conditions. Thermosets made with 1,4-diacetylbenzene-based diketals fully degraded within 8 h while thermosets derived from cyclohexyl and bicyclohexyl diketals required 14–16 h to achieve complete degradation. The most stable thermoset, built from 2,3-butandione-based diketal, required 20 h for complete degradation and showed evidence (*via* comparison with ketal-free control) that ester-hydrolysis may be a competing mechanism of degradation under low pH conditions. At near neutral pH, all thermosets were stable with negligible mass-loss over 120 h. Under basic conditions, all thermosets fully degraded in less than 5 h with profiles that were essentially independent of ketal structure suggesting that ester-hydrolysis is the dominate degradation pathway at high pH. All thermosets exhibited characteristics of surface erosion. Finally, we demonstrated the ability to recover diketones from the thermoset degradation by-products and recycle these compounds into building blocks for additional thermoset materials. The synthetic approach described here for poly

(β-thioether ester ketal) networks should be broadly adaptable to a range of applications (therapeutic delivery, adhesives, *etc*.) requiring materials that undergo full degradation with tunable degradation profiles.

Conflicts of interest

There are no conflicts to declare.

Acknowledgements

The authors gratefully acknowledge financial support from the National Science Foundation (CHE-1710589). BMA acknowledges traineeship support from the NSF Research Traineeship "Interface" program (DGE-1449999) through the University of Southern Mississippi. NGP acknowledges support from the NSF REU Site: Polymer Innovation for a Sustainable Future (DMR-1659340).

Notes and references

1 S. Ma and D. C. Webster, *Prog. Polym. Sci.*, 2018, **76**, 65–110.
2 T. Barrows, *Clin. Mater.*, 1986, **1**, 233–257.
3 S. Binauld and M. H. Stenzel, *Chem. Commun.*, 2013, **49**, 2082–2102.
4 U. Edlund and A. C. Albertsson, in *Degradable Aliphatic Polyesters*, Springer Berlin Heidelberg, Berlin, Heidelberg, 2002, pp. 67–112, DOI: 10.1007/3-540-45734-8_3.
5 S. Hou, D. M. Hoyle, C. J. Blackwell, K. Haernvall, V. Perz, G. M. Guebitz and E. Khosravi, *Green Chem.*, 2016, **18**, 5190–5199.
6 M. S. Rehmann, A. C. Garibian and A. M. Kloxin, *Macromol. Symp.*, 2013, **329**, 58–65.
7 K. L. Poetz, O. Z. Durham and D. A. Shipp, *Polym. Chem.*, 2015, **6**, 5464–5469.
8 B. G. Rutherglen, R. A. McBath, Y. L. Huang and D. A. Shipp, *Macromolecules*, 2010, **43**, 10297–10303.
9 J. Heller, Berlin, Heidelberg, 1993.
10 J. Heller, J. Barr, S. Y. Ng, K. S. Abdellauoi and R. Gurny, *Adv. Drug Delivery Rev.*, 2002, **54**, 1015–1039.
11 V. Bulmus, Y. Chan, Q. Nguyen and H. L. Tran, *Macromol. Biosci.*, 2007, **7**, 446–455.
12 S. Kim, O. Linker, K. Garth and K. R. Carter, *Polym. Degrad. Stab.*, 2015, **121**, 303–310.
13 B. Liu and S. Thayumanavan, *J. Am. Chem. Soc.*, 2017, **139**, 2306–2317.
14 N. Murthy, M. Xu, S. Schuck, J. Kunisawa, N. Shastri and J. M. J. Fréchet, *Proc. Natl. Acad. Sci. U. S. A.*, 2003, **100**, 4995–5000.
15 D. N. Amato, D. V. Amato, Y. Adewunmi, O. V. Mavrodi, K. H. Parsons, S. N. Swilley, D. A. Braasch, W. D. Walker, D. V. Mavrodi and D. L. Patton, *ACS Appl. Bio Mater.*, 2018, **1**, 1983–1991.
16 D. N. Amato, D. V. Amato, O. V. Mavrodi, W. B. Martin, S. N. Swilley, K. H. Parsons, D. V. Mavrodi and D. L. Patton, *ACS Macro Lett.*, 2017, **6**, 171–175.
17 D. V. Amato, D. N. Amato, L. T. Blancett, O. V. Mavrodi, W. B. Martin, S. N. Swilley, M. J. Sandoz, G. Shearer, D. V. Mavrodi and D. L. Patton, *Acta Biomater.*, 2018, **67**, 196–205.
18 D. Huang, F. Yang, X. Wang, H. Shen, Y. You and D. Wu, *Polym. Chem.*, 2016, **7**, 6154–6158.
19 S. Chatterjee and S. Ramakrishnan, *Macromolecules*, 2011, **44**, 4658–4664.
20 M. J. Heffernan and N. Murthy, *Bioconjugate Chem.*, 2005, **16**, 1340–1342.
21 S. Lee, S. C. Yang, M. J. Heffernan, W. R. Taylor and N. Murthy, *Bioconjugate Chem.*, 2007, **18**, 4–7.
22 S. Maity, P. Choudhary, M. Manjunath, A. Kulkarni and N. Murthy, *Chem. Commun.*, 2015, **51**, 15956–15959.
23 H. T. T. Duong, C. P. Marquis, M. Whittaker, T. P. Davis and C. Boyer, *Macromolecules*, 2011, **44**, 8008–8019.
24 E. J. Kepola and C. S. Patrickios, *Macromol. Chem. Phys.*, 2018, **219**, 1700404.
25 E. H. Cordes and H. G. Bull, *Chem. Rev.*, 1974, **74**, 581–603.
26 M. M. Kreevoy, C. R. Morgan and R. W. Taft, *J. Am. Chem. Soc.*, 1960, **82**, 3064–3066.
27 S. D. Khaja, S. Lee and N. Murthy, *Biomacromolecules*, 2007, **8**, 1391–1395.
28 S. Guo, Y. Nakagawa, A. Barhoumi, W. Wang, C. Zhan, R. Tong, C. Santamaria and D. S. Kohane, *J. Am. Chem. Soc.*, 2016, **138**, 6127–6130.
29 E. Schopf, J. Sankaranarayanan, M. Chan, R. Mattrey and A. Almutairi, *Mol. Pharmaceutics*, 2012, **9**, 1911–1918.
30 B. T. Whiting and G. W. Coates, *J. Am. Chem. Soc.*, 2013, **135**, 10974–10977.
31 R. A. Shenoi, B. F. L. Lai, M. Imran ul-haq, D. E. Brooks and J. N. Kizhakkedathu, *Biomaterials*, 2013, **34**, 6068–6081.
32 R. A. Shenoi, J. K. Narayanannair, J. L. Hamilton, B. F. L. Lai, S. Horte, R. K. Kainthan, J. P. Varghese, K. G. Rajeev, M. Manoharan and J. N. Kizhakkedathu, *J. Am. Chem. Soc.*, 2012, **134**, 14945–14957.
33 J. A. Syrett, D. M. Haddleton, M. R. Whittaker, T. P. Davis and C. Boyer, *Chem. Commun.*, 2011, **47**, 1449–1451.
34 K. Srinivasachar and D. M. Neville, *Biochemistry*, 1989, **28**, 2501–2509.
35 S. L. Buchwalter and L. L. Kosbar, *J. Polym. Sci., Part A: Polym. Chem.*, 1996, **34**, 249–260.
36 Y. J. Kwon, S. M. Standley, A. P. Goodwin, E. R. Gillies and J. M. J. Fréchet, *Mol. Pharm.*, 2005, **2**, 83–91.
37 X. Hu, S. Huang, R. Gu, C. Yuan, H. Ge and Y. Chen, *Macromol. Rapid Commun.*, 2014, **35**, 1712–1718.
38 X. Hu, T. Yang, R. Gu, Y. Cui, C. Yuan, H. Ge, W. Wu, W. Li and Y. Chen, *J. Mater. Chem. C*, 2014, **2**, 1836–1843.
39 A. E. Rydholm, S. K. Reddy, K. S. Anseth and C. N. Bowman, *Biomacromolecules*, 2006, **7**, 2827–2836.

40 A. E. Rydholm, C. N. Bowman and K. S. Anseth, *Biomaterials*, 2005, **26**, 4495–4506.
41 A. E. Rydholm, N. L. Held, C. N. Bowman and K. S. Anseth, *Macromolecules*, 2006, **39**, 7882–7888.
42 A. E. Rydholm, S. K. Reddy, K. S. Anseth and C. N. Bowman, *Polymer*, 2007, **48**, 4589–4600.
43 S. Lingier, Y. Spiesschaert, B. Dhanis, S. De Wildeman and F. E. Du Prez, *Macromolecules*, 2017, **50**, 5346–5352.
44 C. E. Hoyle, A. B. Lowe and C. N. Bowman, *Chem. Soc. Rev.*, 2010, **39**, 1355–1387.
45 C. E. Hoyle, T. Lee and T. Roper, *J. Polym. Sci., Part A: Polym. Chem.*, 2004, **42**, 5301–5338.
46 J. Karger-Kocsis, O. Gryshchuk and N. Jost, *J. Appl. Polym. Sci.*, 2003, **88**, 2124–2131.
47 J. Vandenbergh, K. Ranieri and T. Junkers, *Macromol. Chem. Phys.*, 2012, **213**, 2611–2617.
48 J. Vandenbergh, M. Peeters, T. Kretschmer, P. Wagner and T. Junkers, *Polymer*, 2014, **55**, 3525–3532.
49 J. A. Tamada and R. Langer, *Proc. Natl. Acad. Sci. U. S. A.*, 1993, **90**, 552–556.